Quenching the deactivation in the methanol-to-olefins reaction by using tandem fixed-beds of ZSM-5 and SAPO-18 catalysts

José Valecillos[1], Zuria Tabernilla[1], Eva Epelde[1], Enrique Sastre[2], Andrés T. Aguayo[1], Pedro Castaño[1,3*]*

1) Department of Chemical Engineering, University of the Basque Country (UPV/EHU) P.O. Box 644, Bilbao, 48080 Spain

2) Instituto de Catálisis y Petroleoquímica, CSIC, C/Marie Curie, 2, 28049 Madrid, Spain

3) Multiscale Reaction Engineering KAUST Catalysis Center (KCC), King Abdullah University of Science and Technology (KAUST), Thuwal, 23955-6900 Saudi Arabia

* Corresponding authors: jose.valecillos@ehu.eus, pedro.castano@kaust.edu.sa

ABSTRACT: We proved that the disposition of tandem fixed-beds of ZSM-5 with SAPO-18 catalysts could decrease the deactivation of the second catalytic bed during the methanol-to-olefins (MTO) reaction. For this purpose, we prepared two catalysts based on ZSM-5 zeolite and SAPO-18 zeotype; characterized them using XPS, XRD, ^{29}Si NMR, N_2 physisorption, NH_3-TPD and FTIR; tested them individually, in mixed or tandem forms using a fixed-bed reactor or in-situ reactors monitored with UV-vis or FTIR spectroscopies; and characterized the catalyst during the reaction or after it. The catalytic beds (mixed or tandem) did not offer any significant enhancement or synergetic effect in product selectivity. However, the catalytic lifetime of the second bed in the tandem catalytic beds (particularly if that is made up of SAPO-18 catalyst) was prolonged because

this bed receives less oxygenates (methanol and dimethyl ether) and more water, which slows down the deactivation of the second catalytic bed.

1. INTRODUCTION

Light olefins (ethylene, propylene and butylenes) are key building blocks in the petrochemical industry giving way to a vast number of commodities such as polyolefins and other polymers present in our daily life. The main technologies used worldwide for the production of light olefins are steam cracking and fluid catalytic cracking using petroleum derivatives as feedstock. However, China (a big consumer and exporter of commodities) is embracing alternative processes for the production of light olefins from coal via methanol.[1] Despite of the current use of coal (non-renewable resource) as the feedstock, the methanol-to-olefins (MTO) process is constantly claimed to be a prospective alternative for a more sustainable production of light olefins because methanol is obtainable from renewable resources.[2] The MTO reaction needs an acid catalyst to convert oxygenates into hydrocarbons through an autocatalytic dual-cycle mechanism (olefin and aromatic cycles), in which olefins and aromatics are intermediates that act as co-catalysts together with the acid sites for the formation of olefins, aromatics and paraffins.[3–6] The main products are light olefins as long as other products are regarded as side products coming from secondary reactions, such as oligomerization and hydrogen transfer. Furthermore, the degradation of aromatics into large polycyclic

aromatics (coke) is intrinsic to the MTO reaction, which leads to a rapid catalyst deactivation.[4] Thus, two of the main inquiries of the MTO reaction in order to improve the carbon economy of the process are the enhancement of selectivity and prevention of catalyst deactivation, which are strongly related to the catalyst.

The current industrial catalysts for the MTO process are based on the crystalline structures of SAPO-34 zeotypes and ZSM-5 zeolites.[7,8] The SAPO-34 zeotype (CHA structure) is a small-pore material consisting of a perfect arrangement of big cavities (0.67 × 0.11 nm) with small openings (0.38 × 0.38 nm) formed by 8-membered rings.[9] The openings interconnect the cavities and allow the diffusion of only short-chain aliphatics towards the external surface of the crystal, therefore, favoring light olefins selectivity. Its architecture also restricts the size of the polycyclic aromatics formed in the MTO reaction up to 4-ring molecules, which remain trapped in the cavities due to the small openings and consequently leading to a very rapid catalyst deactivation.[10] The SAPO-18 zeotype (AEI structure) is isomorphic to the SAPO-34 zeotype, and is also a potential catalyst for the MTO process.[11–17] The main difference between the architecture of both structures is the orientation of the double-6-rings.[9,18] giving a different shape of the cavities: the AEI

structure shows pear-shaped and wider cavities (larger void volume) at the bottom in comparison with CHA cavities.[11] The differences in the architecture of the cavities determine the formation and reactivity of bulky intermediate species in the MTO reaction,[19] favoring the formation of ethylene and lowering methanol conversion. Furthermore, Gao et al.[20] used pulsed-field gradient nuclear magnetic resonance and molecular dynamics simulations to determine that the differences in the cavity shape of 8-membered rings zeotypes (RHO, CHA and LEV) is crucial for the molecular diffusion throughout the crystals: the higher the cavity size, the higher the rate of molecular diffusion (determined for methane). As a result, SAPO-18 catalysts tend to form more propylene and butylenes than SAPO-34 catalysts, showing high propylene-to-ethylene ratios,[15,21] and to be more resistant to undergo deactivation,[22] which is also attributable to the low concentration of Brønsted acid sites in SAPO-18 zeotypes.[23]

The ZSM-5 zeolite (MFI structure) is a medium-pore material consisting of a three-dimensional structure of 10-membered ring ellipsoidal channels, some straight (0.53 × 0.56 nm) and some in zig-zag (0.51 × 0.55 nm). The similar and constant size of the channels restricts the formation of aromatics to monocyclic and linear polycyclic

aromatics in the MTO reaction and enables the diffusion of some monocyclic aromatics towards the external surface of the crystal. The fact that some monocyclic aromatics leave out the zeolite pores favors the formation of large polycyclic aromatics at the zeolite external surface rather than inside the pores, which prevents the premature blockage of pores and prolongs catalyst lifetime in comparison with small-pore structures.[24] However, the aromatics inside the pores end up forming large linear polycyclic aromatics leading to the imminent catalyst deactivation.[25] The modifications of ZSM-5 zeolites aim to improve light olefins selectivity, and metal and non-metal doping (i.e. B, P, Ca, Cs, Ce, Mg, Ag, Mn, Fe, Ni, Au, Ir, La) is the common strategy reported in the literature.[7,26–32] We recently studied the benefits of modifying ZSM-5 zeolites with $ZnCl_2$ for the MTO reaction at 400 ºC and 1.85 bar. The addition of $ZnCl_2$ balanced the Brønsted and Lewis acid sites, improving propylene selectivity (+10%), decreasing coke formation (-42%) and increasing catalyst lifetime (+80%), which is based on the decrease in the reaction rates of different crucial steps in the MTO reaction.[25]

The abovementioned structural characteristics for small- or medium-pore materials give way to the concept of shape selectivity,[33] which has two faces for the MTO reaction:

improving light olefins selectivity at the expense of a rapid coke accumulation leading to a rapid catalyst deactivation. Based on identical reaction conditions, the comparative study of catalysts with different shape selectivity in the MTO reaction commonly shows that ZSM-5 catalysts are more stable but less selective than SAPO catalysts.[34,35] Other studies focus on bringing together the advantageous properties of two different catalysts by using combined catalysts (including composite or core-shell). In this sense, Qian et al.[36] studied the core-shell composite HZSM-5@SBA-15 in the methanol-to-propylene (MTP) reaction, achieving a high methanol conversion (~98%) and propylene-to-ethylene ratio (~10.7) as well as propylene selectivity (~39%). Xu et al.[10] synthesized SAPO-34@SAPO-18 composites by epitaxial growth method, by providing the composite with a low-silica SAPO-18 shell layer, which suppressed the hydrogen transfer reactions to some extent and improved mass transfer limitations. Thus, they obtained an improved catalytic performance for the MTO reaction at 425 ºC with two times prolonged catalyst lifetime and 9% improvement of light olefins selectivity compared to the parent SAPO-34 catalyst. Smith et al.[11] synthesized a series of SAPO-34/SAPO-18 intergrowths with a range of silicon content from 0.5 to 7.0%. A higher ratio of AEI cages gave a high C_3-C_4

olefins selectivity. This could be explained by the larger size of the AEI cage, which allows the easy diffusion of longer alkenes, as also reported in the literature.[37] Guo et al.[14] also improved the catalytic performance in the MTO reaction (ethylene selectivity of 44% and propylene selectivity of 40%), by using intergrowth CHA/AEI based catalysts at 450 ºC and WHSV= 3 h^{-1}. SAPO-34/ZSM-5 composite catalyst, synthesized by two-step *in-situ* crystallization method, showed an improved catalytic life with a methanol conversion of 97%, and a selectivity of light olefins of 93%.[38] Other authors[39–41] have also reported synergetic effects of SAPO-34/ZSM-5, by adjusting both acid and physical properties (hierarchical mesoporous structure). The benefits are related to higher olefin formation, better dispersion of both phases, increase catalyst site accessibility, due to direct connection of hierarchical matrix structure, as well as improved catalytic lifetime.

In this work, we aim to compare the effect of individual, tandem and mixed beds of ZSM-5 zeolite and SAPO-18 zeotype catalysts for the MTO reaction. For the sake of a fair comparison, we used identical reaction conditions and space times of 0.6 and 1.2 g h mol^{-1}. First, we synthesized two types of catalytic particles based on ZSM-5 or SAPO-18 catalysts, and characterized them by XPS, XRD, ^{29}Si NMR, N_2 physisorption, NH_3-

TPD and FTIR. Second, we analyzed the kinetic performance of the MTO reaction in a fixed-bed reactor with focus on the activity, product distribution and deactivation. We also analyzed in more detail the retained species by performing *in-situ* reactions monitored by Fourier-transform infrared (FTIR) and ultraviolet-visible (UV-vis) spectroscopies. We assessed the performance of the individual, tandem and mixed beds on a kinetic ground.

2. EXPERIMENTAL

2.1. Catalyst preparation

We prepared two catalysts by mixing 50 wt% of an active phase (ZSM-5 zeolite or SAPO-18 zeotype) with 30 wt% of pseudo-boehmite (Sasol, 70 wt% γ-alumina) and 20 wt% of α-alumina (Alfa Aesar, colloidal dispersion at 20% in water), followed by a first drying step at room temperature for 24 h and a second drying step at 110 ºC for 24 h, crushing and sieving at 0.125-0.300 mm, and calcination at 550 ºC for 2 h. We used a ZSM-5 zeolite (Zeolyst International, CBV8014, Si/Al atomic ratio = 40) modified with $ZnCl_2$ (Sigma-Aldrich, 97%) following a procedure described elsewhere,[25] which has a balanced distribution of acid sites that enhances the performance of the MTO reaction. We synthetized the SAPO-18 zeotype by hydrothermal synthesis using diisopropylethylamine (DPEA) as a template[42] with the adaptations proposed by Álvaro-Muñoz et al.,[16] with the following gel composition: $Al_2O_3 : 0.8P_2O_5 : 0.6SiO_2 : 25H_2O : 1.6$DPEA. The reagents used were $Al(OH)_3 \cdot xH_2O$ (Sigma Aldrich, 100%), H_3PO_4 (Sigma Aldrich, 85%), fumed SiO_2 (Degussa, Aerosil), and N,N-diisopropylethylamine (Sigma-Aldrich, 99%). The synthesis procedure consisted of preparing and keeping in agitation a H_3PO_4 solution (6.8 M),

and slowly adding $Al(OH)_3$, SiO_2 and the template in stepwise. The crystallization of the resulting gel took place in a Teflon-lined stainless-steel autoclave vessel at 160 ºC under autogenous pressure for 6 days, using seeds of SAPO-18 crystals provided by Álvaro-Muñoz et al. We recovered the crystallization product by filtration, followed by washing with ethanol and distillated water, drying at 110 ºC for 24 h, and calcination at 550 ºC for 3 h with a heating rate of 5 ºC min^{-1}.

2.2. Catalyst characterization

We used several techniques for characterizing the active phases (zeolites/zeotypes) and catalysts, including X-ray photoelectron spectroscopy (XPS), X-ray diffraction (XRD), solid-state ^{29}Si nuclear magnetic resonance (^{29}Si NMR), N_2 physisorption, NH_3 adsorption and temperature-programmed desorption (NH_3-TPD), and Fourier-transform infrared (FTIR) spectroscopy. Additionally, we analyzed the spent catalysts by using temperature-programmed desorption (TPD) and oxidation (TPO), and extraction of soluble retained species.

The XPS measurements were performed in a SPECS (Berlin, Germany) system equipped with a Phoibos 150 1D-DLD analyzer and a monochromic radiation source of Al Kα (1486.7 eV). The procedure consisted of outgassing a sample of powdered zeolite/zeotype, and pre-scanning for detecting elements present using a step energy of 1 eV, dwell time of 0.1 s and a pass energy of 80 eV. The final scan was based on the elements found using a step energy of 0.1 eV, dwell time of 0.1 s and a pass energy of 30 eV. The fitting software used was CasaXPS 2.3.16 and the spectra were fitted using a Gauss-Lorentzian model after a background subtraction using a Shirley model.

The XRD patterns were measured in a PANalytical Xpert PRO diffractometer equipped with CuKα radiation of 1.5418 Å, using a 2θ step of 0.026° in a 6-60° range. The profile refinement of the diffractogram was performed using the FULLPROF software.

The solid-state ^{29}Si NMR measurements were performed in a Bruker 400 AVANCE III WB spectrometer (9.40T) at a resonance frequency of 79.49 MHz, with a spinning rate of 7 kHz. Cross-polarization measurements were done using a 90° pulse for protons of 3.40 μs, 2.0 ms of contact time, and 5 s of recycle delay. The samples were powdered zeolites/zeotypes and were packed into a cylindrical zirconia rotor (4 mm in outer diameter). The ^{29}Si chemical shifts are referred to $(CH_3)_4Si$.

The N_2 physisorption was performed in a Micromeritics ASAP 2010 apparatus. The procedure consisted of 1) outgassing a sample of 60-120 mg of zeolite/zeotype or catalyst at 150 °C under vacuum (10^{-3} mmHg) for 8 h in order to remove impurities; and 2) N_2 adsorption-desorption in multiple equilibrium steps until sample saturation at 77 K. The analysis of the equilibrium data (isotherms) enabled to calculate the main textural properties using the MicroActive Interactive software. The calculations are based on the Brunauer-Emmett-Teller (BET) method for the total specific surface area or volume and on the t-plot method for the micropore specific surface or volume.

The NH_3 adsorption was performed in a combined thermogravimetry and differential scanning calorimetry (TG-DSC) apparatus (Setaram). The procedure consisted of 1) outgassing a sample of 30-60 mg of zeolite/zeotype or catalyst under He flow at 550 °C for 30 min with a heating rate of 10 °C min^{-1}; 2) cooling down and stabilizing at 150 °C; 3) exposing the sample to 0.05 cm^3 min^{-1} of NH_3 until saturation determined by the stabilization of the thermogravimetric and heat flow signals; and 4) outgassing the NH_3-saturated sample in order to remove the NH_3 physisorbed. The amount of chemisorbed NH_3 is calculated from the thermogravimetric and heat flow experimental data. The NH_3-TPD was performed in a chemisorption analyzer (Micromeritics, AutoChem II 2920). The experimental procedure consisted of 1) outgassing a sample of 60-120 mg of

zeolite/zeotype or catalyst at 20 ºC min^{-1} up to 550 ºC; 2) exposing the sample to NH_3 at 150 ºC as previously described; 3) removing physisorbed NH_3 as previously described; 4) heating up to 550 °C with a heating rate of 5 °C min^{-1} under He flow while analyzing the desorbed NH_3 with a thermal conductivity detector.

The FTIR spectra were measured in a Nicolet 6700 spectrometer (Thermo Scientific) using a high temperature high pressure cell (Specac, HTHP cell). The procedure consisted of 1) pressing a sample of 20 mg of powdered zeolite/zeotype or catalyst and placing it in the cell; 2) outgassing the sample under vacuum at 550 °C for 90 min at a heating rate of 10 °C min^{-1}; 3) cooling down and stabilizing at 400 °C; and 4) collecting spectra by subtracting the background spectrum of the empty cell.

The TPD and TPO of the spent catalysts were performed in a thermobalance (TA Instruments, Q5000) following this procedure described in a previous publication:[25] 1) rapidly outgassing ~15 mg of sample at 200 °C for 20 min in N_2 flow; 2) performing the TPD at a heating rate of 10 °C min^{-1} in 50 cm^3 min^{-1} of N_2 and stabilizing at 550 °C for 1 h; 3) cooling down and stabilizing at 200 °C and switching the flow to air at 50 cm^3 min^{-1}; and 4) performing the TPO at a heating rate of 10 °C min^{-1} and stabilizing at 550 °C for 90 min. The weight loss observed is only attributable to the removal of retained species and coke, and thus the experimental data allow quantifying the coke content.

The extraction of soluble retained species is based on the standard procedure developed by Guisnet and coworkers and adapted as described in a previous publication.[25] Briefly, the experimental procedure consisted of 1) treating ~10 mg of sample in HF (Merck, 40%) with a sample/HF ratio of 10 cm^3 g^{-1} in a Teflon container for 1 h; 2) neutralizing with a NaOH (Panreac, pure) solution; 3) extracting soluble species with 3 cm^3 of dichloromethane (Sigma-Aldrich,

99.8%) by shaking for 1 min; 4) allowing to separate the organic and aqueous phases for 2 h and recovering the organic phase for analysis. We analyzed the organic phase in a gas chromatograph coupled with a mass spectrometer (Shimadzu, GCMS-QP2010S).

2.3. Catalytic tests

We performed kinetic tests for the MTO reaction using a fixed-bed reactor (tubular stainless-steel reactor, inner diameter of 9 mm), using the setup described in a previous publication.[25] The catalytic bed consisted of a mix of catalyst sample (60 or 120 mg) and carborundum (VWR Chemicals, < 0.105 mm) with a total bed volume of 6 cm^3. The experiments consisted of using individual or combined catalytic beds of ZSM-5 and SAPO-18 catalysts. We tested the following combined catalytic beds containing 50 wt% of each catalyst: 1) physical mix of catalyst particles of SAPO-18 and ZSM-5, identified as S+Z; 2) tandem catalytic beds placing the SAPO-18 catalyst on the top, identified as S/Z; and 3) tandem catalytic beds placing the ZSM-5 catalyst on the top (Z/S). For experiments using tandem catalytic beds, we used two beds of 3 cm^3, one containing ZSM-5 catalyst and the other SAPO-18 catalyst and we placed these beds in the reactor separated with a thin layer of glass wool. The typical procedure consisted of 1) outgassing the catalyst in He flow at 550 ºC for 1 h with a heating rate of 10 ºC min^{-1}; 2) cooling down and stabilizing at 400 ºC (reaction temperature); 3) switching the flow to methanol (Sigma-Aldrich, 99.98%) pumped at 0.1 mol h^{-1} and carried with flowing He at a methanol partial pressure of 1.57 bar in a total pressure of 1.85 bar, giving space times of 0.6 or 1.2 g h mol^{-1} according to the catalyst weight; 4) terminating the reaction after observable catalyst deactivation by cutting off the feed and quenching the catalytic bed.

The products were analyzed in gas-vapor phase using a micro-gas chromatograph (Varian, CP4900) with a thermal conductivity detector and three column channels for

simultaneous analysis: 1) Molsieve 5A 8 m length column packed with fumed SiO_2 operated at 45 ºC for the column temperature, 65 ºC for the column injection temperature and 26 psi for the column pressure, for separation of N_2, O_2, CO and CH_4; 2) PoraPLOT Q 10 m length packed column operated at 80 ºC for the column temperature, 80 ºC for the column injection temperature and 26 psi for the column pressure, for separation of C_1-C_4 hydrocarbons and oxygenates; and 3) CP-Sil 5 CB 10 m length packed column operated at 80 ºC for the column temperature, 80 ºC for the column injection temperature and 26 psi for the column pressure, for separation of C_4-C_{10} hydrocarbons a oxygenates. We calculated the conversion (X) assuming that all the identified oxygenates (methanol and dimethyl ether) are reactants in a C-mole basis:

$$X = \frac{F_{M0} - F_M}{F_{M0}} = 1 - Y_M \qquad \text{(Eq. 1)}$$

Where F_{M0} or F_M are the molar flowrates in C-mole basis of oxygenates in the reactor input or output, respectively, and Y_M is the yield of oxygenates in the reactor output. We calculated the yield of a product i (Y_i) or the selectivity of a product i (S_i) on C-mole basis:

$$Y_i = \frac{F_i}{F_{M0}} \qquad \text{(Eq. 2)}$$

$$S_i = \frac{F_i}{F_{M0} - F_M} = \frac{Y_i}{X} \quad \text{(Eq. 3)}$$

Where F_i is the molar flowrate of product i in C-mole basis. We also calculated the catalyst conversion capacity (R_M) defined as the amount of converted oxygenates per catalyst weight during the catalyst lifetime:

$$R_M = \frac{F_{M0} \cdot \overline{X} \cdot t_{0.1}}{W} \quad \text{(Eq. 4)}$$

Where W is the catalyst weight, $t_{0.1}$ is the catalyst lifetime defined as the time on stream at which the conversion decreases down to 10%, and $\overline{X}$ is the average conversion calculated as:

$$\overline{X} = \frac{\int_0^{t_{0.1}} X(t)dt}{t_{0.1} - 0} \quad \text{(Eq. 5)}$$

Where $X(t)$ is the function given by the data of conversion against times on stream (t).

2.3.1. Lifetime frequency

Nash et al.[43] calculated turnover frequencies (TOF) for the ethanol dehydration on acidic catalysts using the total acid site density determined by NH_3-TPD and at steady-state conversions. However, one limitation for utilizing these parameters in the MTO reaction is the unattainable steady-state operation of catalysts due to catalyst deactivation. We attempted to calculate TOFs for modified ZSM-5 catalysts considering the initial conversion measured at various space times under initial conditions and the concentration of Brønsted acid sites,[25] obtaining reasonable values for comparing catalysts in terms of their activity. Dai et al.[44] calculated the TOF for an AlPO-34 catalyst in the MTO reaction at full conversion by determining the accessible density of Brønsted acid sites after a time on stream of 1 h, which avoids the underestimation of the TOF under a full-conversion regime. What they did is to estimate the actual coverage of acid sites at unsaturation

conditions (excess of catalyst), which is a good approach for calculating TOFs for such cases. Rojo-Gama et al.[45] calculated the "conversion capacities" of the MTO reaction on different catalysts in terms of the amount of converted oxygenates during the catalyst lifetime and the concentration of acid sites, which is a quantity (and definition) similar to the TON definition. With these evidences in the literature, we calculated and used the lifetime frequency (*LTF*) defined as the total number of moles of oxygenates converted in one lifetime (down to $X = 0.1$), per mol of acid site and per unit of lifetime:

$$LTF = \frac{\overline{X}}{\left(W/F_{M0}\right) \cdot C_S} \quad \text{(Eq. 6)}$$

Where C_S is the concentration of acid sites in the catalyst determined by NH_3-TPD measurements and W/F_{M0} is the space time used in the experiment.

2.3.2. Fitting model

To make a quantitative assessment of the catalyst deactivation in an integral reactor, we fitted the data of deactivation kinetics to a simple model derived from an ideal fixed-bed reactor mass balance for the oxygenates conversion (X):

$$-r_M = \frac{dX}{d(W/F_{M0})} \quad \text{(Eq. 7)}$$

Where W/F_{M0} is the space time, X is the conversion of oxygenates at any given moment and r_M is the reaction rate at which oxygenates are converted. For simplicity, we considered that oxygenates (M) react with hydrocarbons (H) to form more hydrocarbons, giving rise to an autocatalytic reaction:

$$\mathrm{M} + \mathrm{H} \xrightarrow{k'} \mathrm{H} + \mathrm{H} \quad \text{(Eq. 8)}$$

The material balance based on a C-mole basis gives $C_{M0} = C_M + C_H$ and $C_M = C_{M0}(1 - X)$. Thus, the reaction rate for the conversion of oxygenates can be written as:

$$r = k' C_M C_H a = k(1 - X) X a \quad \text{(Eq. 9)}$$

Where k is the apparent kinetic coefficient for the autocatalytic reaction and a is the activity term that accounts for the catalyst deactivation which varies with time on stream (t). We considered that the change of a with t (da/dt) is independent of any species concentration in the reaction (zeroth order in C_M and C_H), and dependent of a and t according to this empirical expression (see more details in the Supporting Information):

$$-\frac{da}{dt} = k_d a^n t^m \quad \text{(Eq. 10)}$$

Where k_d is the deactivation coefficient. Thus, we solved Eqs. 7 and 9 for X, considering a independent of X and the integration limits ($W/F_{M0} = 0$, $X = X_0$) and ($W/F_{M0} = W/F_{M0}$, $X = X$), giving:

$$X = \frac{b e^{k(W/F_{M0})a}}{1 + b e^{k(W/F_{M0})a}} \quad \text{(Eq. 11)}$$

Where $b = X_0/(1 + X_0)$ is a fitting parameter, found to be 0.01 for all the cases reported in this work, whose meaning is correcting the simple model that omits other reaction steps (such as the conversion of oxygenates into hydrocarbons, M → H). On the other hand, we solved Eq. 10 considering the integration limits ($t = 0$, $a = 1$) and ($t = t$, $a = a$), giving:

$$a = \left[1 - \left(\frac{1 - n}{m + 1}\right) k_d t^{m+1}\right]^{\frac{1}{1-n}} \quad \text{(Eq. 12)}$$

For modelling the case of tandem catalytic beds, we assumed two fixed-bed reactors in series:

$$\frac{W}{F_{M0}} = \frac{W_1}{F_{M0}} + \frac{W_2}{F_{M0}} = \int_{X_0}^{X_1} \frac{dX}{(-r_1)} + \int_{X_1}^{X_2} \frac{dX}{(-r_2)} \quad \text{(Eq. 13)}$$

By using the reaction rate expression for each catalytic bed based on Eq. 9, we can integrate Eq. 13, giving:

$$X_2 = \frac{b^{\frac{k_2 a_2}{k_1 a_1}} e^{(W/F_{M0})k_2 a_2} \left(\frac{X_1}{1-X_1}\right)^{\frac{k_1 a_1 - k_2 a_2}{k_1 a_1}}}{1 + b^{\frac{k_2 a_2}{k_1 a_1}} e^{(W/F_{M0})k_2 a_2} \left(\frac{X_1}{1-X_1}\right)^{\frac{k_1 a_1 - k_2 a_2}{k_1 a_1}}} \quad \text{(Eq. 14)}$$

Where k_1 and a_1 are the kinetic coefficients and activity term of the first catalytic bed, respectively, whose parameters are known from the performance of the corresponding individual catalytic bed; and k_2 and a_2 are the kinetic coefficients and activity term of the second catalytic bed. a_1 and a_2 are obtained using Eq. 12, and we assumed that n and m are the same as those determined from the individual catalytic beds, while k_{d2} is a fitting parameter to be estimated using the experimental data.

2.4. *In-situ* reactions

We performed the MTO reaction in spectroscopic cells monitoring the changes in the catalyst surface by FTIR and ultraviolet-visible (UV-vis) spectroscopies, using the setups described in a previous publication.[25] For the *in-situ* FTIR measurements, we used the same equipment previously described for the FTIR spectra measurements, with the Specac cell functioning as a reactor. For the *in-situ* UV-vis measurements, we used an UV-vis spectrometer (Jasco, V-780) adapted with a special compartment (Jasco, ARN-915i) for using a Linkam cell (THMS600) as a reactor.

The effluent was analyzed using a mass spectrometer (Pfeiffer Vacuum, Omnistar GSD 320 O Series) continuously measuring the m/z signals of 16, 18, 27, 29, 31, 41, 43, 45, 55, 56, 57, 78 and 91. For the experiments, we used individual pressed catalysts of SAPO-18 or ZSM-5 or a pressed catalyst mix of SAPO-18 and ZSM-5 (S+Z) containing 50 wt% of each catalyst. The typical procedure was: 1) outgassing a pressed catalyst sample of 10 mg in N_2 flow at 10 ºC min^{-1} and stabilizing at 550 ºC for 1 h; 2) cooling down and stabilizing at 400 ºC (reaction temperature) for

1 h and collecting background spectra; 3) starting the reaction by switching the feed to a N_2 flow saturated with methanol vapor at 20 ºC and collecting differential spectra (subtracting the background spectrum) continuously at intervals of 35 s (UV-vis spectroscopy) or 2 min (FTIR spectroscopy); and 4) terminating the reaction by cutting off the feed and quenching the catalyst sample by rapidly cooling down the heating element of each cell reactor aided by its respective cooling systems: in the FTIR cell, a Fisons Haake CH chiller with a D8 Fisons Haake controller using a coolant kept at 0-5 ºC, and in the UV-vis cell, a Eheim Professionel 3 circulation pump using cooling water at room conditions.

3. RESULTS

3.1. Catalyst characterization

We used several techniques for characterizing the active phases and catalysts, and these are the main observations:

- The elemental composition analysis using XPS (Table 1) indicates that the ZSM-5 zeolite has a Zn content of 2.19 wt%, whereas the calculated Si/Al atomic ratio is 40.7 (similar to the nominal one). On the other hand, the SAPO-18 zeotype has a nominal Si/(Al + P) atomic ratio of 0.444.
- The XRD patterns of the active phases (Figure 1a) show characteristic peaks with maxima at the indicated diffraction angles (2Θ) for a MFI structure (ZSM-5 zeolite) and an AEI structure (SAPO-18 zeotype).[16,25] Furthermore, we verified the incorporation of Si atoms into the AlPO structure of the synthesized SAPO-18 zeotype by using ^{29}Si NMR (Figure S1 in the Supporting Information), indicating the presence of different $Si(OSi)_x(OAl)_y$ species. However, we infer that the degree of substitution or dispersion

is low on the basis that the band of $Si(OSi)_4$ species is more intense than the bands of $Si(OAl)_4$, $Si(OSi)(OAl)_3$, $Si(OSi)_2(OAl)_2$ and Si(OSi)(OAl) species.

- The SAPO-18 zeotype has more microporous surface than the ZSM-5 zeolite (Table 1) as expected. The corresponding final catalysts have a major proportion of mesoporous surface due to the presence of the added alumina phases,[46] which is expected to enhance the catalyst performance.
- The adsorption of NH_3 indicates that the SAPO-18 zeotype or catalyst have about 2.3 times the concentration of acid sites of the ZSM-5 zeolite or catalyst (Table 1). The dilution of the zeotype or zeolite with the alumina phases to obtain the final catalysts caused a decrease of the concentration of acid sites by about 43%. The acid strength, determined by NH_3-TPD (Figure 1b), is major for the SAPO-18 zeotype than for the ZSM-5 zeolite, with respectively 55 vs 24% of strong-strength acid sites. However, the SAPO-18 and ZSM-5 catalysts have similar distribution of acid sites by their strength: about 48% of strong-strength acid sites and 43% of medium-strength acid sites.
- The nature of acid sites, studied by the vibration of O-H bonds in the 3500-3800 cm^{-1} region in the infrared spectrum (Figure 1c), comprises:[25] bridged Al-OH-Si contributing to Brønsted acid sites (3593 cm^{-1}), aluminols (~3672 cm^{-1}), P-OH species in the SAPO-18 catalyst (~3672 cm^{-1}), silanols (3716 and 3734 cm^{-1}), and aluminols of the added alumina phases (3761 cm^{-1}). As seen, the SAPO-18 catalyst shows less intense 3593 cm^{-1} band than the ZSM-5 catalyst, which is in agreement with the low incorporation of Si atoms in the AlPO structure. In contrast, the SAPO-18 catalyst has a narrow band at 3672 cm^{-1}, indicating the presence of P-OH species that are inferred to account for the high concentration of acid sites and acid strength.

FIGURE 1
TABLE 1

3.2. Individual catalytic beds

Figure 2 shows the evolution of conversion against time on stream for the MTO reaction over ZSM-5 or SAPO-18 catalysts operating at space times of 0.6 or 1.2 g h mol^{-1}. In general, the conversion decreases with increasing times on stream, indicating that the catalysts undergo deactivation. The data show that the conversion decrease is more impactful for the SAPO-18 catalyst regardless of the space time used. The conditions of space time chosen in this work guarantee intermediate and full conversions for evaluating the ZSM-5 catalyst as demonstrated in a previous work;[25] however, these conditions are not appropriate for a stable operation of the SAPO-18 catalyst. The stable operation and extension of the lifetime of SAPO-18 catalysts are doable at space times much higher than those used in this work, e.g. 4.57-32.0 g h mol^{-1}.[16,21,47,48] The rapid deactivation of the SAPO-18 catalyst makes undoable the measurement of the initial conversion for the experiments with this catalyst. The initial conversion, as an indicative of the catalyst activity, is expected to be substantially higher for the SAPO-18 catalyst than for the ZSM-5 catalyst due to the high concentration of acid sites of the SAPO-18 vs ZSM-5 catalysts (0.408 vs 0.176 mmol g^{-1}). The lifetimes (Table 2), defined as the time on stream at which the conversion decreases down to 10% ($t_{0.1}$), are 1.42 or 2.47 h for the SAPO-18 catalyst and 13.3 or 21.0 h for the ZSM-5 catalyst operating at 0.6 or 1.2 g h mol^{-1}, respectively. This quantitatively indicates the rapid deactivation of the SAPO-18 catalyst, and at the same time, evidences the low conversion capacity of this catalyst in comparison with the ZSM-5 catalyst, which is indicated by the area

under the conversion profiles. The estimated conversion capacities (Table 2) are R_M = 0.474 or 0.521 mol g^{-1} for the SAPO-18 catalyst and R_M = 10.7 or 13.8 mol g^{-1} for the ZSM-5 catalyst operating at 0.6 or 1.2 g h mol^{-1}, respectively.

FIGURE 2
TABLE 2

However, not all are disadvantages for the SAPO-18 catalyst. Figure 3 shows one relevant advantage of this catalyst over the ZSM-5 catalyst, which is the high light olefins selectivity obtained from methanol that is a crucial feature for industrial implementations. Firstly, Figure 3a shows the light olefins yield (Y_{LO}) against conversions for both catalysts with lines indicating the selectivity (derived from Eq. 3). As seen, the data for the experiments at different space times of each catalyst overlap indicating the dependence of the yield with the conversion, while the space time only tunes the conversion levels. The light olefins selectivity is ca. 87% and 60% for the SAPO-18 and ZSM-5 catalysts, respectively. Likewise, the light olefins selectivity decreases at high conversions for the ZSM-5 catalyst due to the occurrence of secondary reactions that involve the conversion of light olefins into heavy hydrocarbons, aromatics and paraffins through oligomerization, cyclization and hydrogen transfer reactions (see Figure S2 for a detailed product distribution).[3,49] It is noteworthy to mention that we only observed aliphatic hydrocarbons (mostly olefins) in the reactor output for the experiments using the SAPO-18 catalyst, as reported in other works[16,23,50] (see Figure S2 for a detailed product distribution). This observation is consistence with the severe shape selectivity of the SAPO-18 zeotype,[16] retaining bulky products in the cavities and letting out preferentially short-chain aliphatics.

FIGURE 3

Figures 3b and 3c show the ratios of propylene to ethylene (Y_P/Y_E) and ethylene + propylene to butylenes [$(Y_E + Y_P)/Y_B$] against conversions for a more detailed analysis of the light olefins formation. As seen, the Y_P/Y_E ratio has a poor dependency on the conversion for both catalysts, particularly for the SAPO-18 catalyst, and this ratio is much higher for the SAPO-18 catalyst than for the ZSM-5 catalyst (ca. 2.5-3.0 for the SAPO-18 catalysts vs ca. 1.0-1.5 for the ZSM-5 catalyst). This evidences that the SAPO-18 catalyst favors the formation of propylene over ethylene. On the other hand, the ZSM-5 catalyst shows a clear increasing trend of this ratio with the conversion, making evident that the propylene formation increases with increasing conversions. In contrast, the $(Y_E + Y_P)/Y_B$ ratio has a poor dependency on the conversion for the SAPO-18 catalyst and a strong dependency on the conversion for the ZSM-5 catalyst. This ratio is substantially higher for the ZSM-5 catalyst than for the SAPO-18 catalyst at low conversions, indicating that SAPO-18 catalyst favors the butylenes formation. This ratio decreases with increasing conversions for the ZSM-5 catalyst, and it starts being lower than that of the SAPO-18 catalyst at conversions above 95%. This indicates that the butylenes formation is higher for the ZSM-5 catalyst than for the SAPO-18 catalyst at such high levels of conversion, at which secondary reactions are greatly favored. Butylenes and propylene can be formed from the light olefins oligomerization and subsequent cracking reactions.[3]

Besides, some aromatics are retained in the catalyst, which are partially responsible for the activity of the catalyst and also the main responsible for the catalyst deactivation.[4] We have analyzed these products at different times on stream for the experiments at 0.6 g h mol^{-1} for both

catalysts by using extraction of soluble species, and temperature-programmed desorption (TPD) and oxidation (TPO). The analysis of extracts (Figure S3) indicates that the ZSM-5 catalyst retained only monocyclic aromatics (tetra-, penta- and hexamethylbenzenes), whereas the SAPO-18 catalyst retained monocyclic aromatics (ranging from toluene to hexamethylbenzenes), bi-, tri- and tetracyclic aromatics. Furthermore, we observed that the relative amounts of mono-, bi- or tricyclic aromatics decrease with increasing times on stream for both catalysts, whereas the relative number of tetracyclic aromatics increases with increasing times on stream for the SAPO-18 catalyst. We previously reported this trend for ZSM-5 catalysts, and it was attributable to the evolution of these species into large polycyclic aromatics that are insoluble in dichloromethane.[25] On the other hand, the TPD profiles (Figure S4) show three peaks at 378 ºC, 457-477 ºC and 526 ºC for the ZSM-5 catalyst, and one peak at 477 ºC shifting to 517 ºC with time on stream for the SAPO-18 catalyst. These peaks are attributable to desorption, decomposition and aging of aromatics.[51] In general, the intensity of the TPD peaks (especially those at 378-477 ºC) decreases with increasing times on stream, having a connection with the decrease of the soluble species. The TPO profiles (Figure S4) show one peak at ca. 546 ºC for all the spent catalyst samples, indicating the combustion of coke, and the intensity of this peak increases with increasing times on stream inversely connected with the decrease of the soluble species.

Based on the observations abovementioned, we correlated the relative coke content (calculated from the TPO profiles) with the conversion (Figure 4a) during the MTO reaction over SAPO-18 or ZSM-5 catalysts. The profiles indicate that the relative coke content increases as the conversion decreases, confirming that coke drives catalyst deactivation. For the ZSM-5 catalyst, which has a more complete deactivation profile, it becomes evident that the deactivation process entails three distinguishable steps: (1) the initial buildup of coke in the catalyst causing

insignificant decreases of conversions (high conversions); (2) the stabilization in the coke content at which the conversion decreases significantly; and (3) the final progressive buildup of more coke at the end of the catalytic lifetime (remaining catalytic activity). The last step confirms the fact that coke structure growths due to methylation followed by condensation reactions.[52] For SAPO-18 catalyst, the first step is not observable due to the rapid deactivation of this catalyst, and the coke contents are notoriously higher than those observed for the ZSM-5 catalyst and the methylation/condensation reactions are faster. Figure 4 also depicts the relative abundance of soluble retained species found at 10 min on stream (Figure 4b) and for the deactivated catalyst (Figure 4c). As seen, at the beginning of the reaction (Figure 4b), the SAPO-18 catalyst has more soluble retained species, in a wide range of small polycyclic aromatics, than the ZSM-5 catalyst that only has monocyclic aromatics. When the catalyst has undergone profound deactivation (Figure 4c), the relative abundance of soluble retained species is negligible for the ZSM-5 catalysts, and it is still significant for the SAPO-18 catalyst. It is noteworthy to mention that the relative abundance of mono-, bi- and tricyclic aromatics decreases while that of tetracyclic aromatics increases in the deactivation of the SAPO-18 catalyst.

FIGURE 4

3.3. Combined catalytic beds

In an effort to bring together the advantages of the SAPO-18 and ZSM-5 catalysts, we performed experiments combining both catalysts in a single catalytic bed using the following configurations (showed in Figure 5): 1) tandem catalytic beds placing one catalyst on the top and the other on the bottom (ZSM-5 on the top and SAPO-18 on the bottom, denoted as Z/S, and

SAPO-18 on the top and ZSM-5 on the bottom, denoted as S/Z); and 2) physical mix of particles of both catalysts, denoted as S+Z. In these configurations, the flow is fed at the top of the reactor and we used equal amounts of each catalyst obtaining an overall space time of 1.2 g h mol^{-1}. Figure 5 also shows the conversion against time on stream for these experiments. The S/Z and S+Z combinations show initial conversions above 98%, whereas the Z/S combination shows an initial conversion of ca. 82%. All the combinations show progressive decreases in the conversion indicating progressive catalyst deactivation. The estimated lifetimes ($t_{0.1}$) (Table 2) are 23.1, 18.9 and 18.6 h for the S/Z, S+Z and Z/S configurations, respectively, being notoriously higher than those for the individual SAPO-18 catalyst operating at 0.6 or 1.2 g h mol^{-1} and for the ZSM-5 catalyst operating at 0.6 g h mol^{-1}. The S/Z configuration shows longer lifetime and the Z/S and S+Z configurations show shorter lifetimes than the individual ZSM-5 catalyst operating at 1.2 g h mol^{-1}. The conversion capacities (Table 2) are R_M = 10.3, 8.19 and 7.17 mol g^{-1} for the S/Z, S+Z and Z/S configurations, respectively, being higher than those for the individual SAPO-18 catalyst, and slightly lower than those for the individual ZSM-5 catalyst operating at any space time.

FIGURE 5

Looking at the products obtained using these combined configurations, we observed that the light olefins yield (Y_{LO}) (Figure 6a) and the Y_P/Y_E ratio (Figure 6b) are higher in the configuration order of Z/S > S+Z > S/Z at high conversions, and practically remains the same at low conversions. Similarly, the $(Y_E + Y_P)/Y_B$ ratio (Figure 6c) is slightly lower for the Z/S configuration than low conversions for the S/Z or S+Z configurations. This indicates that the Z/S configuration favors the formation of light olefins (particularly propylene over ethylene) at high conversions and disfavors

the formation of butylenes in the wide range of conversions. In comparison with the individual catalytic beds, the formations of light olefins and propylene are lower than those observed for the SAPO-18 catalyst and are similar to those observed for the ZSM-5 catalyst.

FIGURE 6

We determined the coke content remaining in the catalysts at the end of the experiments and compared them with the individual catalytic beds (Figure 7a). For the tandem catalytic beds, we were able to use the individual catalysts beds. As seen, the coke contents for the ZSM-5 catalysts in the S/Z or Z/S configurations are similar to those observed for the individual ZSM-5 catalyst operating at 0.6 g h mol^{-1} for about 20 h on stream (similar to the operating time of these experiments, ranging 20-23.5 h), and it is much lower than that of the ZSM-5 catalyst operating at 1.2 g h mol^{-1}. On the other hand, the coke contents of the SAPO-18 catalysts in the S/Z and Z/S configurations are higher than those observed in the individual SAPO-18 catalytic bed operating at any space time, which is due to the continuous buildup of coke for the prolonged operating time of the experiments using these configurations (20-23.5 h) in comparison with the experiments using the individual SAPO-18 catalyst (6 h). We also analyzed the retained species at the end of each experiment (Figure 7b), obtaining monocyclic aromatics for both individual catalysts, and small polycyclic aromatics for the SAPO-18 catalysts in the S/Z or Z/S configurations and the mixed S+Z configuration. As seen, the SAPO-18 catalysts in the S/Z or Z/S configurations show much higher relative amounts of retained species than the ZSM-5 catalysts, whereas the S+Z configuration shows an intermediate relative amount of retained species. This result is in

accordance with the study of the individual catalytic beds; the SAPO-18 catalyst is able to retain all the aromatic species whose size is determined by the size of cavities.

FIGURE 7

3.4. Analysis of retained species in *in-situ* reactors

Due to the differences found in the chemistry of retained species in both catalysts, we further studied the nature of retained species in the catalysts under MTO reaction conditions by performing *in-situ* FTIR or UV-vis spectroscopies. When we exposed each catalyst sample to a continuous feed of methanol, we observed the rise of different FTIR bands (Figure 8) or UV-vis bands (Figure 9) due to the formation and retention of hydrocarbons in the catalyst. We explain the assignation of the observed bands in the Supporting Information, based on the literature and extraction of soluble species after each experiment (Figures S5 and S6). As seen, the 1592 and 1379 cm^{-1} bands are the first to rise at the beginning of the reaction (Figure 8a) indicating the formation of small retained species (adsorbed olefins and small aromatics) for all the catalysts. However, after prolonged times on stream (Figure 8b), these bands disappear for the reaction on the ZSM-5 catalyst and are still present for the reaction on the SAPO-18 and S+Z catalysts. All the catalysts show a band at 1570 cm^{-1} (various aromatic species), and the ZSM-5 and S+Z catalysts show a shoulder-band at 1481 cm^{-1} (large polycyclic aromatics or highly condensed coke). On the other hand, the UV-vis spectra (Figure 9) evidences the formation of various monocyclic aromatic carbocations (390 nm) at the beginning of the reaction (Figure 9a) (the band position slightly shifts to 400 nm as seen in Figure 9b) for all the catalysts. The formation of large polycyclic aromatics (592 and 710 nm) is low for the SAPO-18 catalysts in comparison with the

ZSM-5 catalysts, and it is negligible at the beginning of the reaction (Figure 9a), showing only monocyclic aromatic carbocations. The S+Z catalyst sample show all the bands observed for the SAPO-18 and ZSM-5 catalysts with intermediate absorbance intensities.

FIGURE 8
FIGURE 9

4. DISCUSSION

Table 2 lists the results obtained for the *LTF* calculations using the data of the experiments in the fixed-bed reactor (Figures 2 and 5). As seen, the ZSM-5 catalyst has a *LTF* about six times higher than that of the SAPO-18 catalyst in average, despite of the low concentration of acid sites in the former catalyst. The effect of the space time for every individual catalyst is similar: increasing the space time, increases the *LTF*, which may be attributable to an underestimation of the *LTF* for operating with an excess of catalyst. The fact that the *LTF* for the ZSM-5 catalyst is higher than that of the SAPO-18 catalyst relies on the rapid deactivation of the latter catalyst, which shortens the catalyst lifetime and therefore the amount of oxygenates that can be converted (R_M). Figures 4, 8 and 9 confirms the different impacts on the nature and quantity of retained species and coke according to the catalyst morphology: the rapid accumulation of confined retained species (small polycyclic aromatics) in the AEI cavities accelerates the formation of coke and consequently the catalyst deactivation.[21] The overall explanation of such observations may rely on a molecular diffusion phenomenon: as an extrapolation from the work of Gao et al.,[20] it is reasonable to infer that the rate of molecular diffusion of aliphatics is much slower in the SAPO-18 catalyst, which derives in a rapid formation of coke in the SAPO-18 cavities.

For comparing the combined catalytic beds with the individual catalytic beds, we used two approaches. The first approach is based on comparisons at equal total space times (1.2 g h mol^{-1}), which has a more practical outcome for industrial purposes and aims to assess the impact of replacing part of the catalyst with another one while keeping the total catalyst weight in the reactor constant. If the original catalyst is SAPO-18, replacing half of the bed with ZSM-5 catalyst using any configuration leads to a significant improvement on the *LTF* and lifetime ($t_{0.1}$) but with an important decrease on the selectivity (S_{LO}) (Table 2). Conversely, if the original catalyst is ZSM-5, replacing half of the bed with SAPO-18 catalyst leads to low *LTF* and slight improvements on the S_{LO} and $t_{0.1}$. The second approach is based on comparisons at equivalent space times (0.6 g h mol^{-1}) at which the individual catalysts operate in the combined catalytic beds, allowing to understand the results observed. In such situation, the S_{LO} for the experiment using the ZSM-5 catalyst at 0.6 g h mol^{-1} is similar to that of the combined catalytic beds. This indicates that the ZSM-5 catalyst dominates for the selectivity regardless of the presence of the SAPO-18 catalyst whose expected advantage is the improvement on the selectivity. However, the combined catalytic beds have long lifetimes than the individual ZSM-5 catalyst at 0.6 g h mol^{-1}, which indicates a slowdown on the deactivation of at least one of the catalysts in the bed.

We fitted the experimental data combining Eqs. 11 and 12 by adjusting b = 0.01, n and m, and calculating k and k_d. We obtained a satisfactory goodness of fitting by adjusting n = 0 and m = 1/2 for the ZSM-5 catalyst, and n = 7/2 and m = 0 for the SAPO-18 catalyst. This leads to the following set of fitting equations (resulting from combining Eqs. 11 and 12 and substituting the values of b, k, m and n found for each catalyst):

$$X_{\text{ZSM - 5}} = \frac{0.01 \cdot e^{9.209 \cdot \left(W/F_{M0}\right)\left(1 - 0.6667 \cdot k_d t^{3/2}\right)}}{1 + 0.01 \cdot e^{9.209 \cdot \left(W/F_{M0}\right)\left(1 - 0.6667 \cdot k_d t^{3/2}\right)}} \qquad \text{(Eq. 15)}$$

$$X_{\text{SAPO - 18}} = \frac{0.01 \cdot e^{12.68 \cdot \left(W/F_{M0}\right)\left(1 + 2.5 \cdot k_d t\right)^{-2/5}}}{1 + 0.01 \cdot e^{12.68 \cdot \left(W/F_{M0}\right)\left(1 + 2.5 \cdot k_d t\right)^{-2/5}}} \qquad \text{(Eq. 16)}$$

With the kinetic constants being k = 9.209 and 12.68 mol g^{-1} h^{-1} for the ZSM-5 and SAPO-18 catalysts, respectively. For the tandem catalytic beds, we assumed two reactors in series with the behavior of the first catalytic bed known using either Eq. 15 or 16, and we estimated the behavior of the second catalytic bed by using Eq. 14. Table 3 summarizes the calculated parameters and the fitted curves are plotted in Figure 2 or 5. As seen, the k_d of the second catalytic bed decreases with respect to the corresponding catalyst operating in an individual catalytic bed. This decrease is severer for the SAPO-18 catalyst in the Z/S configuration than for the ZSM-5 catalyst in the S/Z configuration. This is due to the low conversion of the SAPO-18 catalyst when is placed in the first catalytic bed (S/Z configuration), so that the input to the second catalytic bed (ZSM-5 catalyst) contains less products and water with more unreacted oxygenates. On the contrary, the high conversions reached in the first catalytic bed (ZSM-5) of the Z/S configuration generates an input to the second catalytic bed (SAPO-18) rich in products and water, causing a great attenuation on the deactivation of the SAPO-18 catalyst. These results indicate that the second catalytic bed is strongly affected by the feed it receives (a mix of unreacted oxygenates, products and water). Co-feeding water with methanol or oxygenates usually slows down catalyst deactivation for ZSM-5 catalysts[53] and SAPO-18 catalysts.[54] The effect of co-feeding water is very pronounced in SAPO-34 catalysts (in similarity with our SAPO-18 catalyst), finding that it can process eight times more methanol than when using a pure feed of methanol.[55] Additionally, we found the best fitting by changing k_2 (the apparent kinetic coefficient of the second catalytic bed), and we explain this on the basis that $k = k'C_{M0}$ (according to Eq. 9), so that k depends on the initial concentration of

reactants (methanol or oxygenates). The initial concentration of reactants to the second catalytic bed decreases and therefore we can expect a decrease on k_2. However, we highlight that our fitting model aimed to estimate deactivation coefficients in order to compare both catalysts, and it did not aim to model the complex kinetics behind the MTO reaction.

5. CONCLUSIONS

We compared the individual and combined (mixed or tandem) beds of SAPO-18 and ZSM-5 catalyst for the methanol-to-olefins reaction. The SAPO-18 catalyst underwent very rapid deactivation due to the retention of polycyclic aromatics blocking the access and diffusion of reactants. The ZSM-5 catalyst suffered much slower deactivation due to its ability to expel single ring aromatics which grow in the meso- and macropores of the catalyst towards highly condensed coke.

Acknowledging the individual advantages of the ZSM-5 and SAPO-18 catalysts, we investigated combined catalytic beds by combining equal amounts of these catalysts in tandem and mixed configurations. The combined catalytic beds can be compared with the individual catalytic beds by using two approaches: 1) on the basis of keeping an equal total catalyst weight in the reactor; and 2) on the basis of comparing with the individual catalytic beds operating at space times similar to the conditions at which each catalyst operates in the configurations. In the former case, the lifetimes and conversion capacities of the combined catalytic beds is significantly improved in comparison with the individual SAPO-18 catalytic bed. In the latter case, the lifetimes of the combined catalytic beds are remarkably improved with respect to both individual catalytic beds. Taking the tandem configurations, the improvements observed in the lifetime are related to the fact that the second catalytic bed processes unreacted oxygenates, products and water, which

modifies the deactivation kinetic. By using the lifetime frequency (*LTF*) and a simple fitting model, we determined that the deactivation (k_d) coefficients of the second catalytic beds are lower than those estimated for the individual catalytic beds operating at similar conditions.

FIGURES

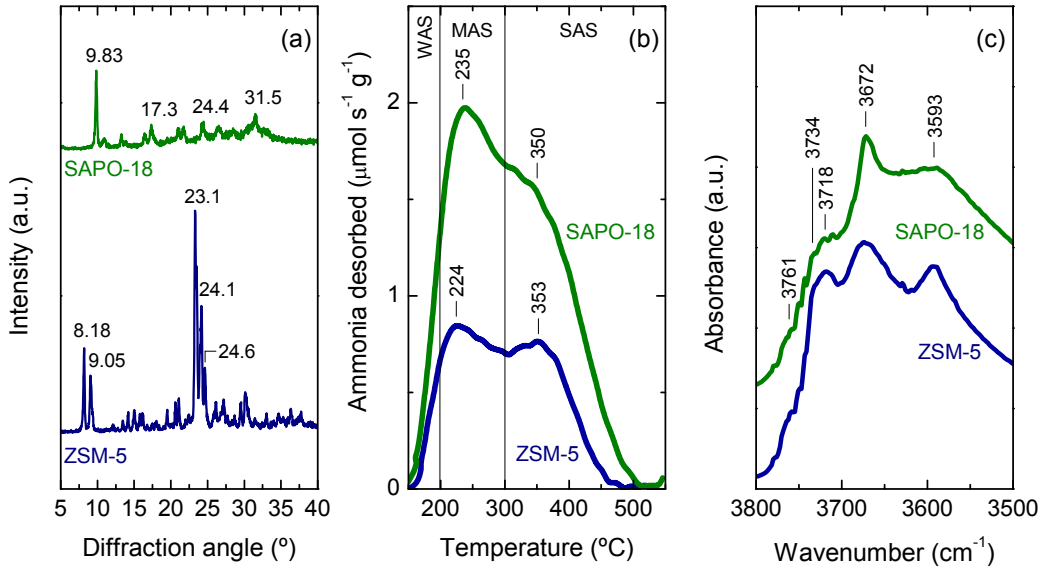

Figure 1. Characterization: (a) XRD patterns of active phases used for catalysts, (b) NH_3-TPD profiles of catalysts, and (c) FTIR spectra in the 3500-3800 cm^{-1} region of catalysts.

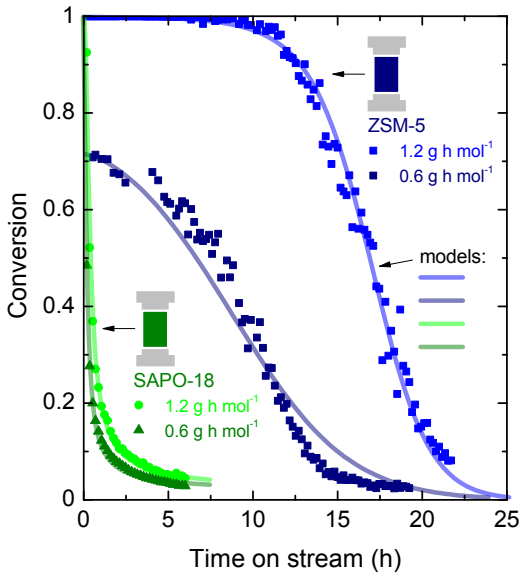

Figure 2. Conversion profiles of individual SAPO-18 and ZSM-5 catalytic beds for the MTO reaction in a fixed-bed reactor. Conditions: T = 400 ºC, W/F_{M0} = 0.6 or 1.2 g h mol^{-1}, $P_{methanol}$ = 1.57 bar.

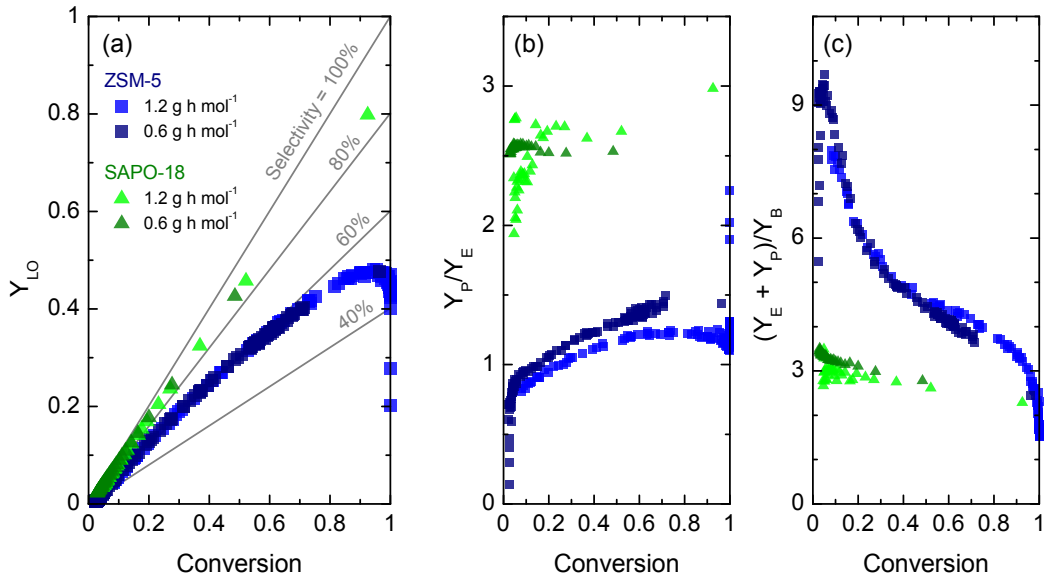

Figure 3. Product distribution profiles of individual SAPO-18 and ZSM-5 catalytic beds for the MTO reaction in a fixed-bed reactor: (a) light olefins yield against conversion, (b) propylene-to-ethylene ratio against conversion, and (c) (ethylene + propylene)-to-butylenes ratio against conversion. Conditions: T = 400 ºC, W/F_{M0} = 0.6 or 1.2 g h mol^{-1}, $P_{methanol}$ = 1.57 bar.

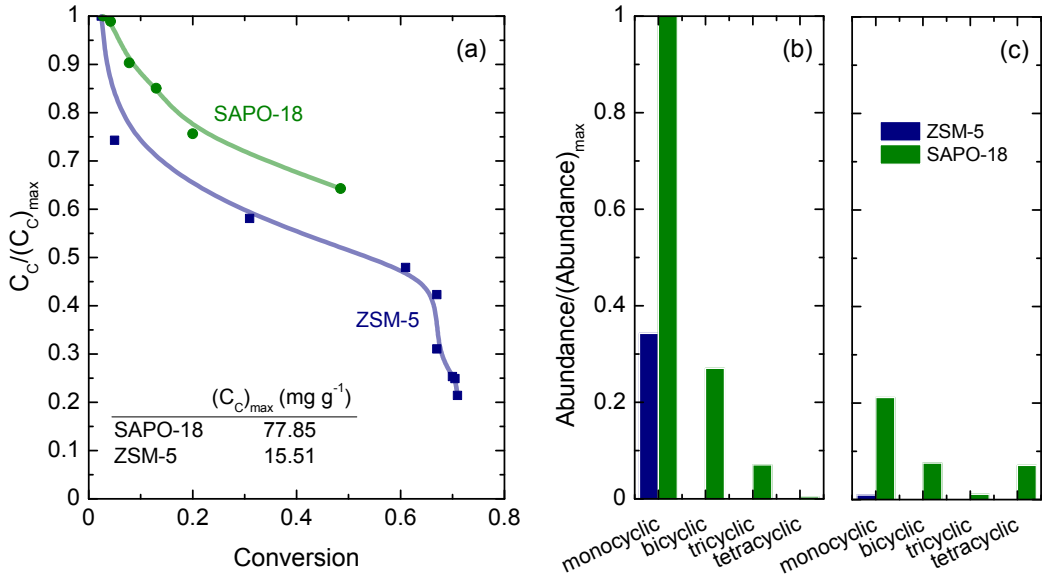

Figure 4. Coking profiles of individual catalytic beds for the MTO reaction in a fixed-bed reactor: (a) evolution of coke content against conversion, and abundance of soluble retained species at (b) 10 min on stream and (c) deactivated catalyst. Conditions: T = 400 ºC, W/F_{M0} = 0.6 g h mol^{-1}, $P_{methanol}$ = 1.57 bar.

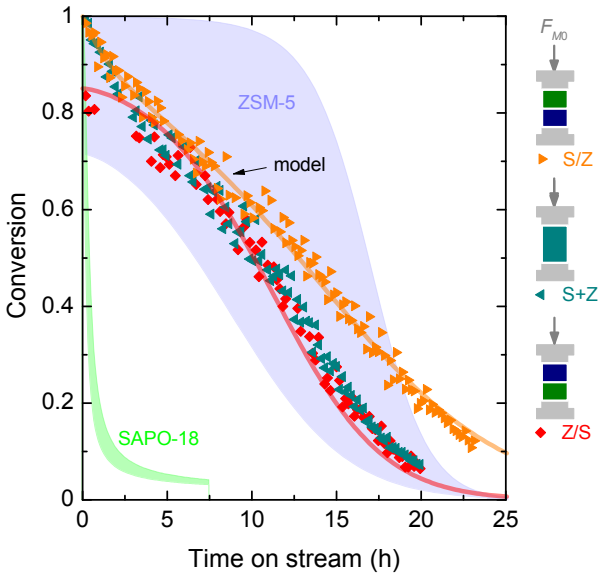

Figure 5. Conversion profiles of combined catalytic beds for the MTO reaction in a fixed-bed reactor. Conditions: T = 400 ºC, W/F_{M0} = 1.2 g h mol^{-1}, $P_{methanol}$ = 1.57 bar.

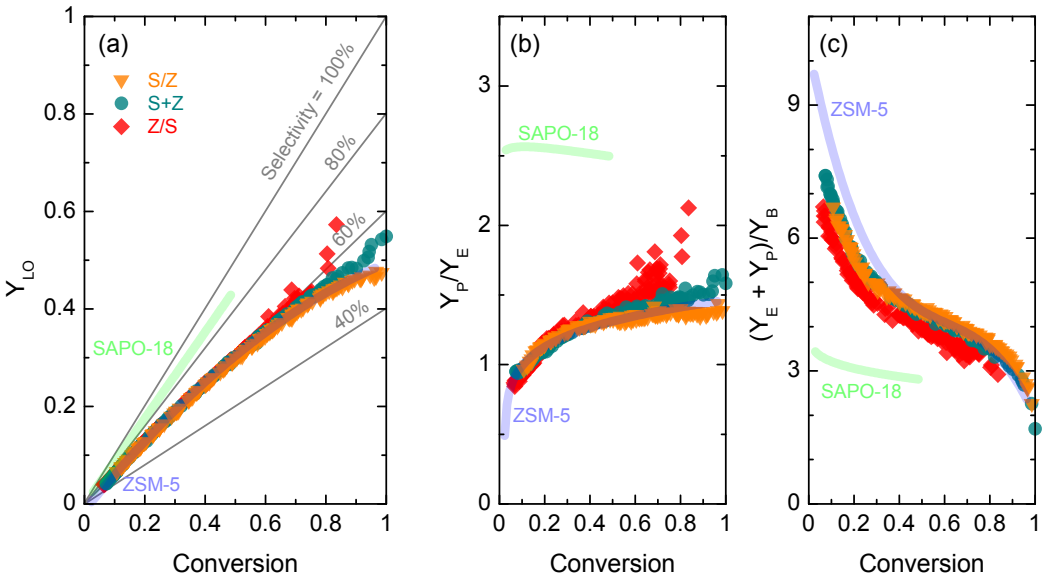

Figure 6. Product distribution profiles of combined catalytic beds for the MTO reaction in a fixed-bed reactor: (a) light olefins yield against conversion, (b) propylene-to-ethylene ratio against conversion, and (c) (ethylene + propylene)-to-butylenes ratio against conversion. Conditions: T = 400 ºC, W/F_{M0} = 1.2 g h mol^{-1}, $P_{methanol}$ = 1.57 bar.

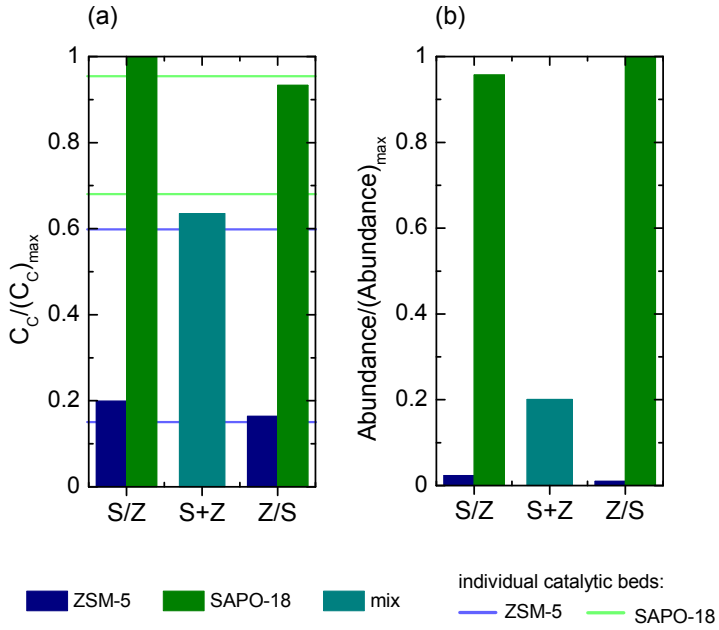

Figure 7. Coke formation in individual and combined catalytic beds for the MTO reaction in a fixed-bed reactor: (a) final coke content, and (b) soluble aromatic species. Conditions: T = 400 ºC, W/F_{M0} = 0.6 or 1.2 g h mol^{-1}, $P_{methanol}$ = 1.57 bar.

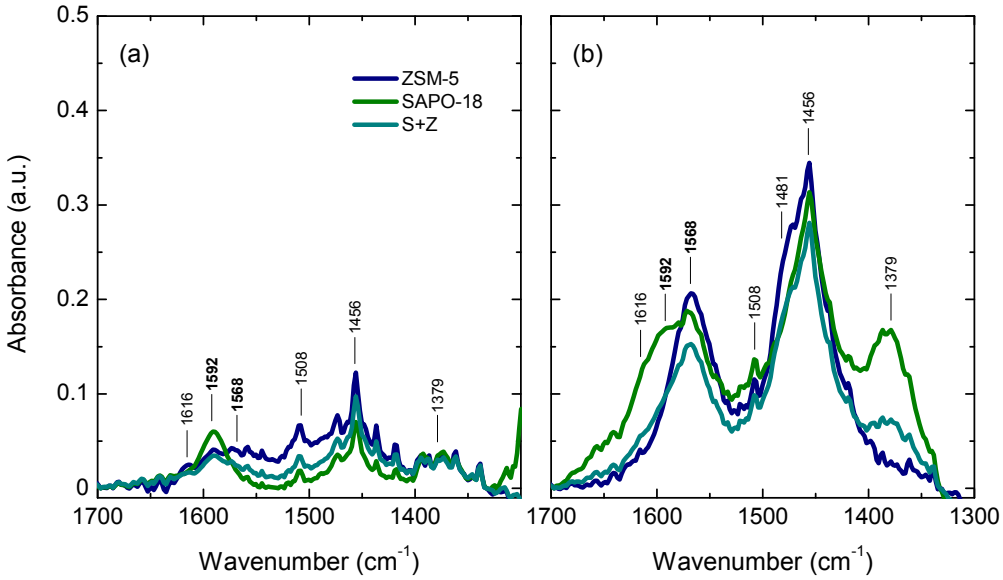

Figure 8. FTIR spectra after the MTO reaction over ZSM-5, SAPO-18 and S+Z catalysts for times on stream of (a) 5 min and (b) 240 min. Conditions: T = 400 ºC, W/F_{M0} = 0.6 g h mol^{-1}, $P_{methanol}$ = 0.16 bar.

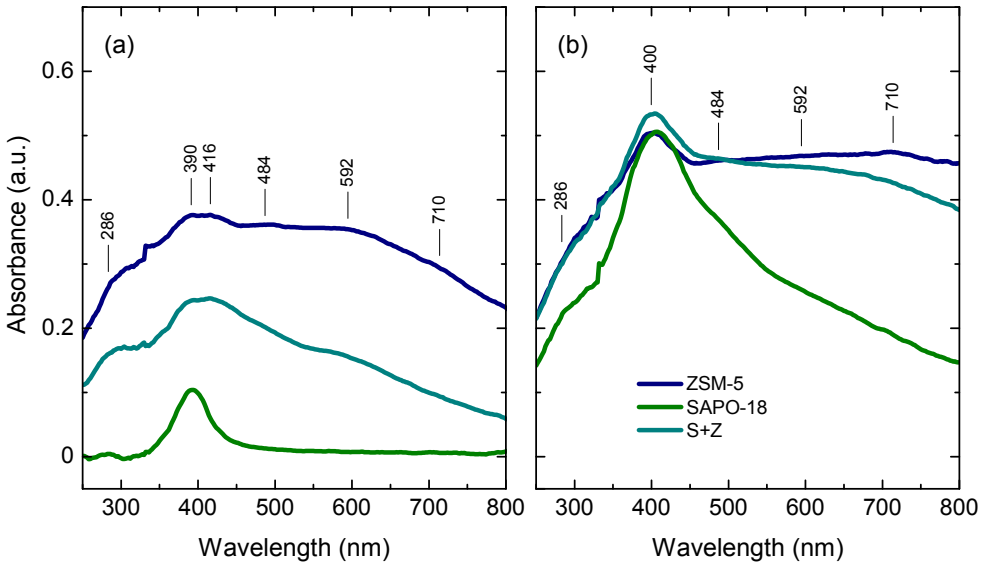

Figure 9. UV-vis spectra after the MTO reaction over ZSM-5, SAPO-18 and S+Z catalysts for times on stream of (a) 5.8 min and (b) 240 min. Conditions: T = 400 ºC, W/F_{M0} = 0.6 g h mol^{-1}, $P_{methanol}$ = 0.16 bar.

TABLES

Table 1. Main properties of active phases and catalysts.

	Zn (wt%)	P (wt%)	Si/(Al+P) (mol mol^{-1})	S_{BET} (m^2 g^{-1})	S_{micro} (m^2 g^{-1})	C_S (μmol g^{-1})	C_{WAS} (μmol g^{-1})	C_{MAS} (μmol g^{-1})	C_{SAS} (μmol g^{-1})
active phases									
ZSM-5	2.19	0	40.7	389	323	311	38.0	198	75.0
SAPO-18	0	17.6	0.444	628	591	718	61.0	262	395
catalysts									
ZSM-5				291	126	176	14.0	77.0	85.0
SAPO-18				353	240	408	28.0	181	199

S_{BET} = specific surface area based estimated using the BET method. S_{micro} = specific surface area of micropores estimated using the t-plot method. C_S = concentration of acid sites estimated from the NH_3 adsorption measurements. C_{WAS}, C_{MAS}, C_{SAS} = concentrations of weak-strength acid sites (WAS), medium-strength acid sites (MAS) and strong-strength acid sites (SAS) estimated from the NH_3-TPD measurements.

Table 2. Activity and deactivation parameters for all the experiments.

Catalytic bed	W/F_{M0} (g h mol^{-1})	R_M (mol g^{-1})	S_{LO}	$t_{0.1}$ (h)	LTF (s^{-1})
ZSM-5	0.6	10.7	60.3	13.3	1.26
	1.2	13.8	51.0	21.0	1.04

SAPO-18	0.6	0.474	88.3	1.42	0.227
	1.2	0.521	86.5	2.47	0.144
S/Z	1.2	10.3	58.0	23.1	0.424
S+Z	1.2	8.19	59.6	18.9	0.412
Z/S	1.2	7.17	61.4	18.6	0.367

W/F_{M0} = space time. R_M = converted oxygenates in the catalyst lifetime. S_{LO} = light olefins selectivity.

Table 3. Fitted parameters using fitting models.

Catalytic bed	W/F_{M0} (g h mol^{-1})	k (mol g^{-1} h^{-1})	k_d (h^{-1})
Individual			
ZSM-5	0.6	9.21	5.97 10^{-2}
SAPO-18	0.6	12.7	7.58
S/Z	1.2		
SAPO-18	0.6	12.7	7.58
ZSM-5	0.6	8.21	3.30 10^{-2}
Z/S	1.2		
ZSM-5	0.6	9.21	5.97 10^{-2}
SAPO-18	0.6	1.38	1.00 10^{-3}

W/F_{M0} = space time. k = kinetic coefficient. k_d = deactivation coefficient.

ASSOCIATED CONTENT

Supporting Information. The following files are available free of charge brief description (file type, i.e., PDF) brief description (file type, i.e., PDF)…

AUTHOR INFORMATION

Corresponding Authors

* jose.valecillos@ehu.eus, * pedro.castano@kaust.edu.sa

Author Contributions

The manuscript was written through contributions of all authors. All authors have given approval to the final version of the manuscript.

ACKNOWLEDGMENT

This work was possible thanks to the financial support of the Ministry of Economy, Industry and Competitiveness of the Spanish Government (Project CTQ2016-79646-P, co-founded with ERDF funds) and the Basque Government (Project IT748-13, IT912-16). J.V. is thankful for his fellowship granted by the Ministry of Economy, Industry and

Competitiveness of the Spanish Government (BES-2014-069980). The authors are thankful for technical and human support provided by IZO-SGI SGIker of UPV/EHU and European funding (ERDF and ESF).

ABBREVIATIONS

a, activity coefficient; a_1, a_2, activity coefficients of first and second catalytic beds; C_C, coke content (wt%); $(C_C)_{max}$, maximum coke content (wt%); C_H, concentration of all hydrocarbons in the reactor; C_M, concentration of all oxygenates in the reactor; C_{M0}, concentration of oxygenates in the reactor's input; C_{MAS}, concentration of medium acid sites (μmol g^{-1}); C_S, concentration of acid sites estimated from NH3 adsorption (μmol g^{-1}); C_{SAS}, concentration of strong acid sites (μmol g^{-1}); C_{WAS}, concentration of weak acid sites (μmol g^{-1}); F_{M0}, molar flowrate of oxygenates in the reactor input (mol h^{-1}); F_M, molar flowrate of oxygenates in the reactor output (mol h^{-1}); k, kinetic coefficient (mol g^{-1} h^{-1}); k_1, k_2, kinetic coefficients of first and second catalytic beds (mol g^{-1} h^{-1}); k_d, deactivation coefficient (h^{-1}); k_{d1}, k_{d2}, deactivation coefficients of first and second beds (mol g^{-1} h^{-1}); $P_{methanol}$, methanol partial pressure (bar); r_M, reaction rate at which

oxygenates are converted (mol g^{-1} h^{-1}); R_M, conversion capacity (mol g^{-1}); S_{BET}, BET specific surface area (m2 g^{-1}); S_i, product selectivity; S_{LO}, light olefin selectivity; S_{micro}, micropore area (m^2 g^{-1}); T, temperature (ºC); t, time on stream (h); $t_{0.1}$, catalyst lifetime (h); W, catalyst mass (g); W/F_{M0}, space time (g h mol^{-1}); X, conversion; X_0, initial conversion; Y_M, yield of oxygenates in the reactor's output; Y_B, butylene yield; Y_E, ethylene yield; Y_{LO}, light olefins yield; Y_P, propylene yield.

LO, light olefins; LTF, lifetime frequency (s^{-1}); MAS, medium acid sites; S/Z, SAPO-18/ZSM-5 tandem bed configuration; S+Z, mixture of SAPO-18+ZSM-5 catalytic bed configuration; SAS, strong acid sites; WAS, weak acid sites; Z/S, ZSM-5/SAPO-18 tandem bed configuration.

REFERENCES

(1) Tian, P.; Wei, Y.; Ye, M.; Liu, Z. Methanol to Olefins (MTO): From Fundamentals to Commercialization. *ACS Catal.* **2015**, *5* (3), 1922.

(2) Olsbye, U.; Svelle, S.; Bjrgen, M.; Beato, P.; Janssens, T. V. W.; Joensen, F.; Bordiga, S.; Lillerud, K. P. Conversion of Methanol to Hydrocarbons: How Zeolite

Cavity and Pore Size Controls Product Selectivity. *Angew. Chemie - Int. Ed.* **2012**, *51* (24), 5810.

(3) Ilias, S.; Bhan, A. Mechanism of the Catalytic Conversion of Methanol to Hydrocarbons. *ACS Catal.* **2013**, *3* (1), 18.

(4) Olsbye, U.; Svelle, S.; Lillerud, K. P.; Wei, Z. H.; Chen, Y. Y.; Li, J. F.; Wang, J. G.; Fan, W. B. The Formation and Degradation of Active Species during Methanol Conversion over Protonated Zeotype Catalysts. *Chem. Soc. Rev.* **2015**, *44* (20), 7155.

(5) Yarulina, I.; Chowdhury, A. D.; Meirer, F.; Weckhuysen, B. M.; Gascon, J. Recent Trends and Fundamental Insights in the Methanol-to-Hydrocarbons Process. *Nat. Catal.* **2018**, *1* (6), 398.

(6) Valecillos, J.; Manzano, H.; Aguayo, A. T.; Bilbao, J.; Castaño, P. Kinetic and Deactivation Differences among Methanol, Dimethyl Ether and Chloromethane as Stock for Hydrocarbons. *ChemCatChem* **2019**, 5444.

(7) Ali, M. A.; Ahmed, S.; Al-Baghli, N.; Malaibari, Z.; Abutaleb, A.; Yousef, A. A Comprehensive Review Covering Conventional and Structured Catalysis for Methanol to Propylene Conversion. *Catal. Letters* **2019**, *149* (12), 3395.

(8) Stöcker, M. Methanol to Olefins (MTO) and Methanol to Gasoline (MTG). In *Zeolites and Catalysis*; Wiley-VCH Verlag GmbH & Co. KGaA: Weinheim, Germany, 2010; Vol. 2, pp 687–711.

(9) Wragg, D. S.; Akporiaye, D.; Fjellvåg, H. Direct Observation of Catalyst Behaviour under Real Working Conditions with X-Ray Diffraction: Comparing SAPO-18 and SAPO-34 Methanol to Olefin Catalysts. *J. Catal.* **2011**, *279* (2), 397.

(10) Xu, Z.; Li, J.; Qian, W.; Ma, H.; Zhang, H.; Ying, W. Synthesis of Core-Shell SAPO-34@SAPO-18 Composites by the Epitaxial Growth Method and Their Catalytic Properties for the MTO Reaction. *RSC Adv.* **2017**, *7* (86), 54866.

(11) Smith, R. L.; Svelle, S.; Del Campo, P.; Fuglerud, T.; Arstad, B.; Lind, A.; Chavan, S.; Attfield, M. P.; Akporiaye, D.; Anderson, M. W. CHA/AEI Intergrowth Materials as Catalysts for the Methanol-to-Olefins Process. *Appl. Catal. A Gen.* **2015**, *505*, 1.

(12) Epelde, E.; Ibáñez, M.; Valecillos, J.; Aguayo, A. T.; Gayubo, A. G.; Bilbao, J.; Castaño, P. SAPO-18 and SAPO-34 Catalysts for Propylene Production from the Oligomerization-Cracking of Ethylene or 1-Butene. *Appl. Catal. A Gen.* **2017**, *547* (March), 176.

(13) Aguayo, A. T.; Gayubo, A. G.; Vivanco, R.; Olazar, M.; Bilbao, J. Role of Acidity and Microporous Structure in Alternative Catalysts for the Transformation of Methanol into Olefins. *Appl. Catal. A Gen.* **2005**, *283* (1–2), 197.

(14) Guo, L.; Zhu, W.; Miao, P.; Li, F.; Guo, Z.; Sun, Q. Intergrowth Silicoaluminophosphate Molecular Sieves Synthesized and Their Catalytic Performances for Methanol to Olefins Reaction. *Ind. Eng. Chem. Res.* **2018**, *57* (31), 10398.

(15) Hunger, M.; Seiler, M.; Buchholz, A. In Situ MAS NMR Spectroscopic Investigation of the Conversion of Methanol to Olefins on Silicoaluminophosphates SAPO-34 and SAPO-18 under Continuous Flow Conditions. *Catal. Letters* **2001**, *74* (1–2), 61.

(16) Álvaro-Muñoz, T.; Márquez-Álvarez, C.; Sastre, E. Mesopore-Modified SAPO-18

with Potential Use as Catalyst for the MTO Reaction. *Top. Catal.* **2016**, *59* (2–4), 278.

(17) Chen, J.; Li, J.; Yuan, C.; Xu, S.; Wei, Y.; Wang, Q.; Zhou, Y.; Wang, J.; Zhang, M.; He, Y.; et al. Elucidating the Olefin Formation Mechanism in the Methanol to Olefin Reaction over AlPO-18 and SAPO-18. *Catal. Sci. Technol.* **2014**, *4* (9), 3268.

(18) Wendelbo, R.; Akporiaye, D.; Andersen, A.; Dahl, I. M.; Mostad, H. B. Synthesis, Characterization and Catalytic Testing of SAPO-18, MgAPO-18, and ZnAPO-18 in the MTO Reaction. *Appl. Catal. A Gen.* **1996**, *142* (2), 197.

(19) Li, J.; Wei, Y.; Chen, J.; Xu, S.; Tian, P.; Yang, X.; Li, B.; Wang, J.; Liu, Z. Cavity Controls the Selectivity: Insights of Confinement Effects on MTO Reaction. *ACS Catal.* **2015**, *5* (2), 661.

(20) Gao, S.; Liu, Z.; Xu, S.; Zheng, A.; Wu, P.; Li, B.; Yuan, X.; Wei, Y.; Liu, Z. Cavity-Controlled Diffusion in 8-Membered Ring Molecular Sieve Catalysts for Shape Selective Strategy. *J. Catal.* **2019**, *377*, 51.

(21) Chen, J.; Li, J.; Wei, Y.; Yuan, C.; Li, B.; Xu, S.; Zhou, Y.; Wang, J.; Zhang, M.; Liu, Z. Spatial Confinement Effects of Cage-Type SAPO Molecular Sieves on Product Distribution and Coke Formation in Methanol-to-Olefin Reaction. *Catal. Commun.* **2014**, *46*, 36.

(22) Marcus, D. M.; Song, W.; Ng, L. L.; Haw, J. F. Aromatic Hydrocarbon Formation in HSAPO-18 Catalysts: Cage Topology and Acid Site Density. *Langmuir* **2002**, *18* (22), 8386.

(23) Chen, J.; Thomas, J. M.; Wright, P. A.; Townsend, R. P. Silicoaluminophosphate Number Eighteen (SAPO-18): A New Microporous Solid Acid Catalyst. *Catal. Letters* **1994**, *28* (2–4), 241.

(24) Epelde, E.; Ibáñez, M.; Aguayo, A. T.; Gayubo, A. G.; Bilbao, J.; Castaño, P. Differences among the Deactivation Pathway of HZSM-5 Zeolite and SAPO-34 in the Transformation of Ethylene or 1-Butene to Propylene. *Microporous Mesoporous Mater.* **2014**, *195*, 284.

(25) Valecillos, J.; Epelde, E.; Albo, J.; Aguayo, A. T.; Bilbao, J.; Castaño, P. Slowing

down the Deactivation of H-ZSM-5 Zeolite Catalyst in the Methanol-to-Olefin (MTO) Reaction by P or Zn Modifications. *Catal. Today* **2019**, *348*, 243.

(26) Yaripour, F.; Shariatinia, Z.; Sahebdelfar, S.; Irandoukht, A. Effect of Boron Incorporation on the Structure, Products Selectivities and Lifetime of H-ZSM-5 Nanocatalyst Designed for Application in Methanol-to-Olefins (MTO) Reaction. *Microporous Mesoporous Mater.* **2015**, *203* (C), 41.

(27) Tian, S. X.; Ji, S. F.; Sun, Q. Preparation of Phosphorus Modified HZSM-5 Zeolite Catalysts and Their Catalytic Performances of Methanol to Olefins. In *Advanced Materials Research*; Trans Tech Publications Ltd, 2014; Vol. 875–877, pp 295–299.

(28) Yarulina, I.; Bailleul, S.; Pustovarenko, A.; Martinez, J. R.; Wispelaere, K. De; Hajek, J.; Weckhuysen, B. M.; Houben, K.; Baldus, M.; Van Speybroeck, V.; et al. Suppression of the Aromatic Cycle in Methanol-to-Olefins Reaction over ZSM-5 by Post-Synthetic Modification Using Calcium. *ChemCatChem* **2016**, *8* (19), 3057.

(29) Gorzin, F.; Yaripour, F. Production of Light Olefins from Methanol over Modified H-ZSM-5: Effect of Metal Impregnation in High-Silica Zeolite on Product Distribution.

Res. Chem. Intermed. **2019**, *45* (2), 261.

(30) Khezri, H.; Izadbakhsh, A.; Izadpanah, A. A. Promotion of the Performance of La, Ce and Ca Impregnated HZSM-5 Nanoparticles in the MTO Reaction. *Fuel Process. Technol.* **2020**, *199* (August 2019), 106253.

(31) Rostamizadeh, M.; Yaripour, F.; Hazrati, H. Ni-Doped High Silica HZSM-5 Zeolite (Si/Al = 200) Nanocatalyst for the Selective Production of Olefins from Methanol. *J. Anal. Appl. Pyrolysis* **2018**, *132* (April), 1.

(32) Goetze, J.; Weckhuysen, B. M. Spatiotemporal Coke Formation over Zeolite ZSM-5 during the Methanol-to-Olefins Process as Studied with *Operando* UV-Vis Spectroscopy: A Comparison between H-ZSM-5 and Mg-ZSM-5. *Catal. Sci. Technol.* **2018**, *8* (6), 1632.

(33) Teketel, S.; Erichsen, M. W.; Bleken, F. L.; Svelle, S.; Lillerud, K. P.; Olsbye, U. *Shape Selectivity in Zeolite Catalysis. The Methanol to Hydrocarbons (MTH) Reaction*; 2014; Vol. 26.

(34) Mohammadkhani, B.; Haghighi, M.; Aghaei, E. Enhanced Stability and Propylene Yield in Methanol to Light Olefins Conversion over Nanostructured SAPO-34/ZSM-5 Composite with Various SAPO-Loadings. *Asia-Pacific J. Chem. Eng.* **2019**, *14* (1), 1.

(35) Jang, H. G.; Min, H. K.; Lee, J. K.; Hong, S. B.; Seo, G. SAPO-34 and ZSM-5 Nanocrystals' Size Effects on Their Catalysis of Methanol-to-Olefin Reactions. *Appl. Catal. A Gen.* **2012**, *437–438*, 120.

(36) Qian, X.; Du, J.; Li, B.; Si, M.; Yang, Y.; Hu, Y.; Niu, G.; Zhang, Y.; Xu, H.; Tu, B.; et al. Controllable Fabrication of Uniform Core-Shell Structured Zeolite@SBA-15 Composites. *Chem. Sci.* **2011**, *2* (10), 2006.

(37) Chang, N.; Bai, L.; Zhang, Y.; Zeng, G. Fast Synthesis of Hierarchical CHA/AEI Intergrowth Zeolite with Ammonium Salts as Mineralizing Agent and Its Application for MTO Process. *Chem. Pap.* **2019**, *73* (1), 221.

(38) Wu, H.; Wang, X.; Liu, F.; Cao, J. Facile in Situ Hydrothermal Crystallization Synthesis of SAPO-34/ZSM-5 Composite Catalyst for Methanol to Olefin Reaction.

J. Porous Mater. **2018**, *26* (3), 793.

(39) Chae, H. J.; Song, Y. H.; Jeong, K. E.; Kim, C. U.; Jeong, S. Y. Physicochemical Characteristics of ZSM-5/SAPO-34 Composite Catalyst for MTO Reaction. *J. Phys. Chem. Solids* **2010**, *71* (4), 600.

(40) Liu, F.; Wang, X.; Xu, F.; Lin, Q.; Pan, H.; Wu, H.; Cao, J. Fabrication and Characterization of Composites Comprising (CHA)SAPO-34 with (MFI)ZSM-5 Topologies and Their Catalytic Performances on MTO Reaction. *Microporous Mesoporous Mater.* **2017**, *252*, 197.

(41) Moradiyan, E.; Halladj, R.; Askari, S. Beneficial Use of Ultrasound in Rapid-Synthesis of SAPO34/ZSM-5 Nanocomposite and Its Catalytic Performances on MTO Reaction. *Ind. Eng. Chem. Res.* **2018**, *57* (6), 1871.

(42) Meier, W. M. AEI SAPO-18a Al(49), P(42), Si(9). In *Verified Syntheses of Zeolitic Materials*; Elsevier, 2001; Vol. 98, pp 81–83.

(43) Nash, C. P.; Ramanathan, A.; Ruddy, D. A.; Behl, M.; Gjersing, E.; Griffin, M.; Zhu,

H.; Subramaniam, B.; Schaidle, J. A.; Hensley, J. E. Mixed Alcohol Dehydration over Brønsted and Lewis Acidic Catalysts. *Appl. Catal. A Gen.* **2016**, *510*, 110.

(44) Dai, W.; Wang, X.; Wu, G.; Li, L.; Guan, N.; Hunger, M. Methanol-to-Olefin Conversion Catalyzed by Low-Silica AlPO-34 with Traces of Brønsted Acid Sites: Combined Catalytic and Spectroscopic Investigations. *ChemCatChem* **2012**, *4* (9), 1428.

(45) Rojo-Gama, D.; Signorile, M.; Bonino, F.; Bordiga, S.; Olsbye, U.; Lillerud, K. P.; Beato, P.; Svelle, S. Structure–Deactivation Relationships in Zeolites during the Methanol-to-Hydrocarbons Reaction: Complementary Assessments of the Coke Content. *J. Catal.* **2017**, *351*, 33.

(46) Pérez-Uriarte, P.; Gamero, M.; Ateka, A.; Díaz, M.; Aguayo, A. T.; Bilbao, J. Effect of the Acidity of HZSM-5 Zeolite and the Binder in the DME Transformation to Olefins. *Ind. Eng. Chem. Res.* **2016**, *55* (6), 1513.

(47) Martínez-Franco, R.; Li, Z.; Martínez-Triguero, J.; Moliner, M.; Corma, A. Improving the Catalytic Performance of SAPO-18 for the Methanol-to-Olefins (MTO) Reaction

by Controlling the Si Distribution and Crystal Size. *Catal. Sci. Technol.* **2016**, *6* (8), 2796.

(48) Xu, Z.; Li, J.; Qian, W.; Ma, H.; Zhang, H.; Ying, W. Synthesis of Core-Shell SAPO-34@SAPO-18 Composites by the Epitaxial Growth Method and Their Catalytic Properties for the MTO Reaction. *RSC Adv.* **2017**, *7* (86), 54866.

(49) Chang, C. D.; Silvestri, A. J. The Conversion of Methanol and Other O-Compounds to Hydrocarbons over Zeolite Catalysts. *J. Catal.* **1977**, *47*, 249.

(50) Gayubo, A. G.; Vivanco, R.; Alonso, A.; Valle, B.; Aguayo, A. T. Kinetic Behavior of the SAPO-18 Catalyst in the Transformation of Methanol into Olefins. *Ind. Eng. Chem. Res.* **2005**, *44* (17), 6605.

(51) Castaño, P.; Ruiz-Martínez, J.; Epelde, E.; Gayubo, A. G.; Weckhuysen, B. M. Spatial Distribution of Zeolite ZSM-5 within Catalyst Bodies Affects Selectivity and Stability of Methanol-to-Hydrocarbons Conversion. *ChemCatChem* **2013**, *5* (10), 2827.

(52) Schulz, H. “Coking” of Zeolites during Methanol Conversion: Basic Reactions of the MTO-, MTP- and MTG Processes. *Catal. Today* **2010**, *154* (3–4), 183.

(53) Gayubo, A. G.; Aguayo, A. T.; Atutxa, A.; Prieto, R.; Bilbao, J. Role of Reaction-Medium Water on the Acidity Deterioration of a HZSM-5 Zeolite. *Ind. Eng. Chem. Res.* **2004**, *43* (17), 5042.

(54) Gayubo, A. G.; Aguayo, A. T.; Alonso, A.; Atutxa, A.; Bilbao, J. Reaction Scheme and Kinetic Modelling for the MTO Process over a SAPO-18 Catalyst. *Catal. Today* **2005**, *106* (1–4), 112.

(55) Wu, X.; Anthony, R. G. Effect of Feed Composition on Methanol Conversion to Light Olefins over SAPO-34. *Appl. Catal. A Gen.* **2001**, *218* (1–2), 241.

TABLE OF CONTENT